Crystal chemistry, structure and magnetic properties of the Cu(Mo,W)O4 solid solution series.

Bjoern Christian Schwarz, Helmut Ehrenberg, Hans Weitzel, Anatoliy Senyshyn, Brunhilde Thybusch, Michael Knapp, Garry James Mcintyre, Hartmut Fuess

Crystal chemistry, structure and magnetic properties of the Cu(Mo,W)O4 solid solution series.

Journal:	*Philosophical Magazine & Philosophical Magazine Letters*
Manuscript ID:	TPHM-07-Oct-0283.R1
Journal Selection:	Philosophical Magazine
Date Submitted by the Author:	20-Feb-2008
Complete List of Authors:	Schwarz, Bjoern; IFW Dresden, Institute for complex materials Ehrenberg, Helmut; IFW Dresden, Institute for complex materials Weitzel, Hans; TU Darmstadt, Structural Research Senyshyn, Anatoliy; TU Darmstadt, Structural Research Thybusch, Brunhilde; TU Darmstadt, Chemical Analytics Knapp, Michael; CELLS, Alba McIntyre, Garry; Institute Laue Langevin Fuess, Hartmut; TU Darmstatd, Structural Research
Keywords:	diffraction, magnetic oxides, magnetic structure, transmission electron microscopy
Keywords (user supplied):	diffraction, magnetic oxides, magnetic structure

Note: The following files were submitted by the author for peer review, but cannot be converted to PDF. You must view these files (e.g. movies) online.

abstract.tex
cover.tex
paper_acc.tex
figures.tex
tables.tex

Philosophical Magazine,
Vol. 00, No. 00, DD Month 200x, 1–16

Crystal chemistry, structure and magnetic properties of the $Cu(Mo_x W_{1-x})O_4$ solid solution series.

B. SCHWARZ†*, H. EHRENBERG†, H. WEITZEL‡, A. SENYSHYN‡, B. THYBUSCH‡, M. KNAPP§, G.J. MCINTYRE¶, H. FUESS‡

†Institute for Complex Materials, IFW Dresden, Helmholtzstrasse 20, D-01099 Dresden, Germany
‡Institute for Materials Science, Darmstadt University of Technology, Petersenstrasse 23, D-64287 Darmstadt, Germany
§CELLS, P. O. Box 68, 08193 Barcelona, Spain
¶Insitut Max von Laue – Paul Langevin, 6 rue Jules Horowitz, BP. 156X, 38042 Grenoble Cedex 9, France

(released october 2007)

For a solid solution series the common description of a crystal as a homogeneous solid formed by a repeating, three-dimensional pattern of a unit cell is in principle no longer applicable, taking the statistical chemical distribution of the substituting ions into account. The $Cu(Mo_xW_{1-x})O_4$ solid solution series represents an appropriate system to investigate how this chemical distribution affects the details of the crystal structure: Due to different coordination preferences of the isovalent diamagnetic ions W and Mo, a decisive magnetic exchange path couples ferromagnetically in $CuWO_4$, but antiferromagnetically in the isostructural compound $CuMoO_4$-III. From the investigations of the magnetic properties of the solid solution series it can be inferred for a certain range of stoichiometries that the Mo/W cation disorder of the solid solution series does not result in a corresponding disordered distribution of magnetic coupling constants but in a formation of a super structure of them. The magnetic superexchange here acts as a very sensitive probe for local bonding geometries. Consequently, in the solid solution cooperative structural processes dominate over individual coordination preferences. In the present work $Cu(Mo_xW_{1-x})O_4$ powder samples are characterized with high resolution synchrotron diffraction, magnetization measurements and neutron diffraction. $Cu(Mo_xW_{1-x})O_4$ single crystals are characterized by electron probe micro analysis, transmission electron microscopy, x-ray structure refinement and profile analyses, magnetization measurements and diffraction with 'white' and monochromatic neutrons.

1 Introduction

The effect of structural distortions on the magnetic super exchange coupling [1] can exclusively be investigated by pressure dependent experiments providing quantitative information about the magnetic exchange parameters. Metal organic compounds consisting of magnetically decoupled dimers (or polymers of lower order) and containing weakly interacting metal centres usually represent relative simple magnetic systems that were subject to those considerations, experimentally as well as theoretically [2]. Contrary to that, in the current work the effect of geometrical distortion on the magnetic coupling in an inorganic crystal that builds up a three dimensional long range magnetic order below a critical transition temperature is investigated. Here the structural changes are not induced by an external pressure, but by the substitution of diamagnetic isovalent ions differing to a very small extent in how they are coordinated by surrounding atoms. While the end members, corresponding to a complete substitution of these ions, can correctly be described as a homogeneous solid formed by a repeating, three-dimensional pattern of a unit cell, this concept is in principal not applicable for the partial substitution of the solid solution series taking into account that each site is occupied either by one ion or the other in a statistical manner. The question is, whether the chemical variation on an atomic length scale will lead to a variation in local geometry depending on the specific occupation by the sort of the diamagnetic ion, or if correlated processes are dominating in a crystal resulting in a kind of averaged structure. Since the magnetic super- and super superexchange interactions are very sensitive on variations of the local geometry, the realized magnetic properties of the solid solution series will give information concerning this question of fundamental interest

*Corresponding author. Email: b.schwarz@ifw-dresden.de

Philosophical Magazine
ISSN 1478-6435 print/ISSN 1478-6443 online © 200x Taylor & Francis
http://www.tandf.co.uk/journals
DOI: 10.1080/1478643YYxxxxxxxx

for understanding solid solutions.

Due to a unique combination of properties, the $Cu(Mo_xW_{1-x})O_4$ solid solution series represents an appropriate system for this purpose. The magnetic Cu^{2+} ions have spin $\frac{1}{2}$ and the series' end members have different, but rather simple collinear antiferromagnetic ground state structures with no temperature dependend magnetic phase transitions. Since the system is electronically insulating at low temperatures its electrons are highly localized and therefore local structural changes only affect the superexchange properties of the direct atomic vicinity. The decisive magnetic J_1(B) coupling path changes from being ferromagnetic in $CuWO_4$ to antiferromagnetic in the isostructural compound $CuMoO_4$-III due to different coordination preferences of the diamagnetic ions W and Mo. The type of local coordination, i.e. more W-like or more Mo-like, determines the type of local magnetic coupling, i.e. ferro- or antiferromagnetically, respectively. Conversely the magnetic properties, since depending strongly on the spatial distribution of ferro- respectively antiferromagetic coupling paths, will provide information on the spatial distribution of rather W-like respectively Mo-like coordination in crystals of the solid solution series. The mutual substitution of the isovalent diamagnetic ions does not alter the valency of the magnetic Cu ions, but has only structural effects.

The $Cu(Mo_xW_{1-x})O_4$ solid solution series is introduced in more detail in the following. The compounds $MeWO_4$ (Me = Mn [3], Fe [4], Co [5], Ni [6]) crystallize in the monoclinic $P2/c$ wolframite structure with both types of metal atoms situated on twofold axes. The irregular coordination of copper induced by the Jahn-Teller [7] effect breaks the twofold symmetry, and $CuWO_4$ crystallizes in a triclinic distorted wolframite-type structure with space group $P\bar{1}$ [8][1]. In all compounds cis-edge-sharing CuO_6 octahedra form infinite CuO_4 zigzag chains that run along the c direction and are corner connected with infinite MeO_4 zigzag chains that are formed by MeO_6 octahedra. The $MeWO_4$ series with Me = Co, Ni, Fe and Cu exhibits long-range antiferromagnetic order at low temperature with a magnetic propagation vector $\vec{k}_W=(\frac{1}{2}, 0, 0)$ [25,26]. $CuWO_4$ orders collinear antiferromagnetically below 23.0(2) K with an ordered magnetic moment of 0.67(1) μ_B per copper ion at 2 K [22]. The direction of the magnetic moments coincides, within the experimental uncertainty, with the axes of elongation of the Jahn-Teller distorted octahedra of oxygen atoms coordinating the Cu^{2+} ions. At high pressure and high temperature α-$CuMoO_4$ [27] undergoes a phase transition to $CuMoO_4$-III that is isostructural to $CuWO_4$ and remains metastable when the pressure is released after cooling to room temperature [28–31]. The same structure is also observed for the mixed oxides $Cu(Mo_xW_{1-x})O_4$ with more W than Mo [32]. The small structural changes induced by the complete substitution of the diamagnetic W ions by the isovalent Mo ions result in the formation of another type of magnetic ordering. $CuMoO_4$-III orders collinear antiferromagnetically below 31(1) K, but in contrast to $CuWO_4$, with the magnetic propagation vector $\vec{k}_M=(0, 0, \frac{1}{2})$ [32].

In previous studies a low-temperature neutron diffraction study of $Cu(Mo_xW_{1-x})O_4$ powder samples prepared by subsolidus reaction was performed [33]. For each of the two mixed compounds with averaged Mo contents of 0.25 and 0.35 the magnetic $CuMoO_4$-III- as well as the magnetic $CuWO_4$-type have been found coexisting at 1.5 K. The coexistence of these two magnetic arrangements is interpreted in [33] as reflecting an inhomogeneous distribution of Mo and W in different crystallites together with a sharp transition between the stability ranges of the two types of magnetic structures at a determinate stoichiometry $x_d \approx 0.28$. The specific Mo:W distributions in the crystallites of the powdered samples were deduced from a profile analysis based on high-resolution synchrotron powder diffraction data and confirmed the strong inhomogeneity of the powder samples prepared by subsolidus reaction.

Due to the observed inhomogeneity, the evolution of the magnetic structure upon the increase of the Mo-content cannot be revealed with the necessary accuracy and stoichiometric resolution. Therefore, in this work $Cu(Mo_xW_{1-x})O_4$ powder samples are not prepared by subsolidus reaction but by the wet chemical Pechini route and in addition also $Cu(Mo_xW_{1-x})O_4$ single crystals are grown by chemical transport. The powder samples are characterized by high resolution synchrotron x-ray diffraction (XRD), magnetization measurements and neutron powder diffraction. The single crystals are characterized by electron probe micro analysis (EPMA), single crystal XRD and profile analysis, transmission electron microscope (TEM),

[1]Beside the investigations on crystal growth [9] [10], optical, electrical and electrochemical characteristics [11–13], hydrogen reduction [14], photoelectrochemical investigations [15,16] etc. also the magnetic properties of $CuWO_4$ were investigated extensively [17–24].

TEM energy dispersive x-ray analysis (EDX), magnetization measurements and diffraction with 'white' and monochromatic neutrons.

2 Sample preparation, experiments and results

2.1 *Powder samples*

2.1.1 ***Preparation.*** The powder samples were synthesized by the Pechini method [34]: Ammonium tungsten oxide pentahydrate ($(NH_4)_{10}W_{12}O_4{\cdot}5H_2O$, Puratronic®, 99.999 %) and ammonium molybdate tetrahydrate ($(NH_4)_6Mo_7O_{24}{\cdot}4H_2O$, Puratronic®, 99.999 %) with a specific Mo/W ratio are dissolved to high concentration in distilled water. Citric acid forms complexes with the metal cations, preventing the direct precipitation of Cu-W-Mo-O compounds, when appropriate amounts of copper(II)nitrate hemi(pentahydrate) ($Cu(NO_3)_2{\cdot}2.5H_2O$) in aqueous solution are added. At this stage all cations are solved very homogeneously in a liquid solution. The solvent is slowly evaporated and at a certain level the citric acid polycondensates and forms a foam. The organic content is removed by a pyrolysis reaction and the so obtained precursor is transformed to $Cu(Mo_xW_{1-x})O_4$ with the distorted wolframite-type structure by heating for three days at 963 K as described in [33]. The homogeneous cation distribution of the liquid solution is assumed to be 'frozen in' and preserved in the solid state promising much more homogeneous samples than those prepared by subsolidus reaction.

2.1.2 ***Cation distribution function.*** Representative analyses of the cation distributions in the samples are obtained by Rietveld refinements [35] based on high-resolution synchrotron diffraction data measured at the beamline B2 at the Hamburger Synchrotron Strahlungslabor (Germany). The distribution function has been approximated by refining the scale factors for up to 13 phases in steps of $\Delta x = 0.05$ starting from $x = 0$, on the basis of the half-width and profile parameters deduced from a LaB_6 standard as a reference and with specific lattice parameters obtained from a linear interpolation between those for $CuMoO_4$-III and those for $CuWO_4$, see table 4. The same atomic parameters have been used for all phases; only the Mo and W site occupation factors were adapted to x for each phase individually and kept fixed during the refinement. The observed half-widths of the reflections are mainly determined by the variation of the angles γ and α, because contributions like particle size and stress effects would follow different characteristic dependences on 2θ, which can unambigously separated from a broadening caused by a specific distribution of lattice parameters. This feature can be illustrated by comparison of the half-width for the 020- and $1\bar{1}1$-reflection: Whereas the position of the first one is nearly independent on the Mo-content, the position of the latter varies strongly with Mo-content, leading to a very narrow 020- and a very broad $1\bar{1}1$-reflection in the case of very inhomogeneous samples. As an example, for an average Mo-content of $<x> = 0.25$ sections of observed and calculated diffraction patterns for a sample prepared by subsolidus reaction (top) as well as for one prepared by the Pechini method (bottom) are opposed in figure 1. The direct comparison of the half-widths of the $1\bar{1}1$-reflections indicates that the Pechini sample is much more homogeneous. This fact is quantified by the plot of the scale factors of the discrete compositions used to approximate the continuous cation distribution function, presented in figure 2. For higher Mo-contents $<x> = 0.30$, 0.35 and 0.50 the $1\bar{1}1$-reflection is anomalously broadened towards smaller values of 2θ with respect to the 020-reflection, as indicated with arrows in figure 3. This means that the Mo/W ratio in a particular small part of the crystallites has decreased. Since the amount of the Mo-rich γ-$Cu(Mo_xW_{1-x})O_4$ phase [36] increases in proportion to the averaged Mo content, it can be deduced that the profile anomalies are caused by an inhomogeneous formation of the γ-$Cu(Mo_xW_{1-x})O_4$ phase affecting mainly those crystallites with a higher Mo-content within the cation distribution function. This diffusion controlled phase transition can partially be suppressed by higher cooling rates after the heating, outlined in the next chapter about the magnetization measurements.

2.1.3 ***Magnetization measurements.*** Since the main $Cu(Mo_xW_{1-x})O_4$ phase with distorted wolframite-type structure orders three dimensionally antiferromagnetic whereas the second phase γ-$Cu(Mo_xW_{1-x})O_4$ exhibits paramagnetic behaviour until down to low temperatures [36], magnetization measurements at low temperature are a very sensitive probe for detecting smallest amounts of the latter phase. Whereas samples with $<x> = 0.25$ prepared by the Pechini method do not show a strong dependence of the magnetic properties on the cooling rate, i.e. there is no noticable amount of the paramagnetic second phase in either case, the difference for the sample with $<x> = 0.35$ becomes more pronounced. Here a dramatic increase of magnetization when approaching low temperature indicates the existence of the paramagnetic γ-$Cu(Mo_xW_{1-x})O_4$ phase when the sample was cooled down slowly during preparation. With a higher cooling rate the diffusion controlled formation of that phase can be suppressed and the corresponding magnetization curve is typical for a pure antiferromagnetic sample of this type of compound [24]. Consequently, in order to obtain samples that do not lose Mo to a second phase, all samples used for the subsequent measurements were quenched in air after heating. The amount of the second phase is not only a matter of thermal treatment of the sample but also of the preparation method itself. As mentioned above for the Pechini samples with $<x> = 0.25$ even the samples that were cooled down slowly did not contain a paramagnetic second phase, whereas the sample with the same Mo-content prepared by subsolidus reaction contains paramagnetic contributions. For a variety of stoichiometries magnetization vs. temperature was measured and the Néel temperatures were extracted as the temperature of highest slope (figure 4). All samples prepared by the Pechini method order antiferromagnetically with Nel temperatures not below 19 K, and there is no remarkable difference to the corresponding results of the samples prepared by subsolidus reaction.

2.1.4 ***Neutron powder diffraction.*** Samples with $<x> = 0$, 0.25, 0.30 and 0.35 were prepared by the Pechini method and quenched in air after heating for three days at 963 K. Each sample was measured for about 24 hours at the neutron powder diffractometer SPODI (FRM II, München, Germany). Beside the main $Cu(Mo_xW_{1-x})O_4$ phase, traces of γ-$Cu(Mo_xW_{1-x})O_4$ and WO_3 could be observed, but to much smaller extent in comparison to the samples prepared by subsolidus reaction. For a comparative evaluation both datasets, one measured at DMC on the sample prepared by subsolidus reaction [33], the other measured at SPODI on the Pechini sample, were analyzed in the same manner by the Rietveld method [35,37]. For the chemical structure of the $Cu(Mo_xW_{1-x})O_4$ main phase the Mo/W ratio was fixed to the nominal averaged value, whereas the scale factor, the profile parameters, the cell parameters and the isotropic displacement factors were refined [1]. For the description of the magnetic phase the direction of the magnetic moment of 0.67(1) μ_B was restrained to lie along the Jahn-Teller elongated axis of the CuO_6-octahedron. For $CuWO_4$, this was determined by neutron diffraction on a single crystal [22] and the Rietveld refinement based on neutron powder diffraction on $CuMoO_4$-III with retention of the same moment direction resulted in an ordered magnetic moment of the same magnitude ($0.67(3)\mu_B$) [32]. All refined magnetic scale factors are related to the normalized scale factors of the particular chemical main phase that builds up the magnetic structure. Table 4 presents the sum of the scale factors of the $CuWO_4$-type ($\frac{1}{2}$, 0, 0) and the $CuMoO_4$-III-type (0, 0, $\frac{1}{2}$) magnetic structure related to the normalized nuclear scale factor and futhermore the relative amount of the latter magnetic structure in relation to the sum of both. Consistent with the data presented in [33], that is given here again in square brackets, the amount of $CuMoO_4$-III-type magnetic material (related to the sum of both magnetic structure types) increases from 42(11) % [40 %] for $<x> = 0.25$ to 67(16) % [70 %] for $<x> = 0.35$. It should be emphasized that the magnetic reflections are very weak and the scale factors have large standard deviations. Firstly the results for the samples prepared by the Pechini method are discussed: The end member $CuWO_4$ ($<x> = 0$) orders completely (104(11) %) in the $CuWO_4$-type magnetic structure as expected. The relative amount of the $CuMoO_4$-III-type magnetic structure for $<x> = 0.25$, 0.30, 0.35 is 48(9) %, 65(14) %, 85(29) %, respectively, reflecting the increasing Mo-content at least qualitatively. The sums of the scale factors of both magnetic structure types related to the nuclear scale factor are in the same stoichiometrical order

[1] only the most important parameters are mentioned here.

36(13) %, 30(16) % and 11(9) %. That means that only some part of the Cu(Mo$_x$W$_{1-x}$)O$_4$ phase with distorted wolframite-type structure orders magnetically in one of the end member magnetic structures. These results are clearly pronounced for the Pechini samples, also by taking the relatively large standard deviations into consideration, whereas the samples prepared by subsolidus reaction show this behaviour only to a minor extend. As an illustration, in figure 5 the part of the neutron diffractogram where the two strongest magnetic reflections $\frac{1}{2}$ 0 0 (CuWO$_4$-type) and 0 0 $\frac{1}{2}$ (CuMoO$_4$-III-type) are presented for a variety of stoichiometries for the Pechini and the subsolidus samples. All diffractograms are normalized to the same nuclear scale factor and shifted a little bit in the y direction for clarity. The integral intensity of the reflections is of course not equally proportional to the scale factor, since the magnetic structure factor is considerably different for the two reflections of the two magnetic structures.

2.2 *Single crystals*

2.2.1 ***Preparation.*** The crystals were synthesized by chemical transport. For CuWO$_4$ the crystal growth by chemical transport is described in [38]. In this work single crystals were grown from Cu(Mo$_x$W$_{1-x}$)O$_4$ charges (prepared by subsolidus reaction) by chemical transport in a quartz ampoule in a two zone furnace. The largest Cu(Mo$_x$W$_{1-x}$)O$_4$ crystals were obtained using approximately 3 mg/cm^3 tellurium chloride as transport agent and a nominal temperature gradient of 50 K between the charge (1083 K) and crystallizing zone (1023 K) over a length of 200 mm. In accordance with the results in [38] also in this work it was not possible to synthesize pure CuWO$_4$ by chemical transport, but only by recrystallization. Consequently, the presence of Mo seems to support crystallization by chemical transport.

2.2.2 ***Electron probe micro analysis.*** A large Cu(Mo$_x$W$_{1-x}$)O$_4$ crystal ($2.0 \cdot 2.0 \cdot 0.7$ mm^3) was cut into slices and the surfaces of the so obtained slices were wet polished with decrescent graining down to 1 μm. The polished surface guarantees that the x-ray signal is only correlated to the chemical composition and not to the topology of the surface roughness. The electron probe micro analysis was performed on a 'Cameca sx50' with an acceleration voltage of 20 kV, a current of 20 nA and a resting time of approximately 3 minutes per measuring point. The beam diameter on the surface is approximately 1 μm and the information depth is up to several micrometers.

A tungsten-metal, molybdenum-metal, copper-metal and a silica standard are used for the calibration of the quantitative analyses of tungsten, molybdenum, copper and oxygen, respectively. Table 4 gives the x-ray lines used for the quantification and the corresponding energies. The stoichiometry x is calculated for different measuring points on the polished crystal surface by the ratio of the given atomic Mo-concentration divided by the sum of the atomic Mo- and W-concentration. SE-images for each surface allow for the verification, that none of the measuring points is situated within a pore or likewise imperfection. Exemplarily for a large number of measurements, figure 6 (left) presents the results of a line scan over a whole crystal surface showing clearly fluctuations of the Mo-concentration. On a length scale from 350 to 400 μm the stoichiometry x is nearly constant, but changes abruptly from about $x = 0.25$ to 0.35 in an alternating manner. The other crystal surface slices also show variations in the Mo-content to the same extend, but the alternating scheme is most pronounced for the presented one. The line scan is used in order to evaluate the correctness of the measured Mo-concentrations. Therefore, the corresponding atomic concentrations of the elements tungsten, molybdenum, copper and oxygen are presented in figure 6 (right). The crucial result is that the concentrations of tungsten and molybdenum counteract, whereas those of copper and oxygen remain nearly constant. This is the expected behaviour of the substitutional Cu(Mo$_x$W$_{1-x}$)O$_4$ solid solution series and shows clearly that the observed fluctuations of the Mo-concentrations are a real effect. The fact that the sum of the unconstrained element concentration is indeed approximately equal to 100 % for all measured points indicates that there is no additional impurity in a significant amount. The observed Mo distribution topology with abrupt changes of the concentration can be explained neither by local nor by temporal gradients during crystal growth as reported for metallic Mo/W-system [39]. Investigations in dependence of the temper treatment promote that this kind of Mo/W distribution is already built up during crystal growth. The formation of abruptly changing concentrations is for example also known for

the high-T_c-superconductors $R_{2-x}Ce_xCuO_4$ (R = Pr, Nd, Sm, Eu) grown from a melt-solution. Since the lattice parameters depend on the stoichiometry x these inhomogeneities result in a splitting and/or broadening of certain diffraction reflections [40–42] as is also found for the present system (see below). Due to the different growth methods the suggested explanation for the formation of the inhomogeneities in the crystal given in [40] cannot be transferred to the present work and remain ambiguous for the $Cu(Mo_xW_{1-x})O_4$ crystals grown by chemical transport.

2.2.3 ***X-ray profile analysis.*** The x-ray profile analysis was performed on a 4-circle diffractometer from STOE. The Co x-ray tube was operated with a voltage of 40 kV and a current of 35 mA. The Co-K_α-line consists of the Co-$K_{\alpha1}$- and the Co-$K_{\alpha2}$-line with an intensity ratio of approximately 2:1. An averaged wavelength of $\lambda_{av} = 1.7902$ Å was used. In order to obtain bulk information about the Mo distribution, the $Cu(Mo_xW_{1-x})O_4$ crystal ($70 \cdot 150 \cdot 350$ μm^3) was broken into several pieces and single crystal x-ray structure refinements were performed on each of the pieces, after the crystal as a whole was analysed with regard to its x-ray line profile. Since the crystal pieces were rather large the absorption correction is not perfect and therefore the estimated standard deviations (given in brackets) are rather high. The Mo-content varies from $x = 0.24(2)$ up to $x = 0.55(5)$ in five individual pieces, i.e. even stronger than expected from the surface sensitive analysis. Figure 7 shows the high resolution volume q-scans of the 200-, $0\bar{2}0$- and the 002-reflections. The datapoints are represented in an orthonormal basis. The edge length of the volumes in reciprocal space are only about 0.04 of the corresponding reciprocal basis vector. In order to illustrate the intensity distribution $I(h,k,l)$ the volumes are intersected by a grid with a resolution of $\Delta h/\Delta k = 0.002$. The intensities from $I_{max}/30$ and $I_{max}/2$ are divided in ten equidistant sections that are encoded into colours and presented on the planes. The $0\bar{2}0$-reflection is obviously broadened or even shows indications of a splitting along the reciprocal a^* direction compared to the 200- and 002-reflections. For a further characterization of this phenomenon the 400-, $0\bar{4}0$-, 004-, 130- and 220-reflections are measured in addition and presented in figure 8. The 400- and 004-reflections clearly exhibit a visible splitting along the a^* and the c^* direction, respectively, that is due to the coexistence of $CoK_{\alpha1}$ and $CoK_{\alpha2}$, resulting in a splitting along the direction through the reciprocal origin. In contrast, the large broadening of the $0\bar{4}0$-reflection (note the enlarged section) is again in a^* direction and cannot be explained due to $CoK_{\alpha1}$ and $CoK_{\alpha2}$. Especially the fact, that also the 130- and 220-reflections containing $0k0$-contributions, show splitting, proves the existence of more than one crystal metrics with different parameters and excludes the possibility to explain the profiles by the superposition of any desired rotation of two or more identical crystal metrics. All profiles can be explained by a common and fixed direction of the c^* and the a^* axis over the whole crystal and a varying direction of the b^* axis mainly in the b^*-a^*-plane. Consequently, in real space this means that only the a axis changes its direction within the b-a-plane, i.e. mainly the angle γ changes due to varying Mo-content. This is in agreement with the metric parameters variations as a function of the Mo-content x, obtained from a linear interpolation of the end members, given in table 4. The single crystal x-ray structure refinement of the crystal pieces of different stoichiometry revealed a maximal verifiable difference of the bulk Mo-content of about $\Delta x = 0.30$ corresponding to a change of γ of approximately $\Delta\gamma \approx 0.42°$. In the approximation of an orthonormal coordinate system a rotation of the reciprocal point 020 within the b^*-a^*-plane of $\Delta\gamma \approx 0.42°$ results in a displacement of about 0.015 in a^* direction, which is in good agreement with the actually found broadening of the $0\bar{2}0$-reflection.

2.2.4 ***Transmission electron microscopy.*** For TEM investigations a thin-section sample of another large $Cu(Mo_xW_{1-x})O_4$ crystal was produced by first cutting a slice of approximately 1 mm thickness out of a crystal that was further thinned by wet polishing with decrescent graining. When reaching a thickness of about 50 μm the polishing was stopped and the crystal was further thinned by ion milling with Argon.

All investigations were performed with a PHILIPS CM 20 transmission electron microscope with an applied voltage of 200 kV. Apart from the electron micro probe analysis, the homogeneity of the Mo-distribution was also investigated by energy dispersive x-ray (TEM-EDX) analysis.

For the quantification of the Mo-content x both, the ratio of the intensities of the Mo_L- and W_M- as well as that of the Mo_K- and W_L-line, obtained by measuring each point for about 10 minutes, were utilized.

A multitude of measuring points are distributed over rather small areas of $1 \cdot 1$ μm^2, $5 \cdot 5$ μm^2, and $100 \cdot 100$ μm^2. The Mo-content for these measuring points is constant within the uncertainty of $\Delta x \approx \pm 0.02$.

In bright field TEM mode a multitude of of discontinuous line shaped regions with enhanced scattering contrast is observable. In order to get more insight into the origin of the imperfections causing the contrast, figure 9 shows a high resolution bright field image of one of the imperfections (left), a horizontal compression of an image of the same imperfection to 10 % (middle) and a magnification thereof (right). Marking a (010) lattice plane well above and below the imperfection, where the crystal is essentially undisturbed, and counting the number of lattice planes between these lines right and left from the imperfection results in one plane more on the left side than on the right side at a total number of 70 planes. Consequently, this appears as a kind of antiphase boundary, especially in the middle of the imperfection (figure 9 (right)). Only a minority of the crystal regions showing that enhanced scattering contrast can be ascribed to that kind of crystal distortion. For the majority of imperfections showing the same sort of scattering contrast the crystal distortions are less pronounced. The more detailed investigation reveals that the contrast is caused by the misaligned coincidence of different crystal domains.

Beside this kind of imperfection another type exists appearing as a weak line-shaped scattering contrast along the a direction. Its origin is a crystal domain with a specific twin relation to the surrounding crystal (figure 10). The spatial extension in a direction does not exceed 50 nm, but reaches up to several 100 nm in b direction. The image is taken along the [00±1] direction that is maintained throughout all domains, whereas the a and b axes are rotated by a two-fold axis parallel to the b axis at the transition from one domain to the other. These facts are further supported by the twinning analysis of the single crystal investigation presented below.

2.2.5 ***Magnetization and heat capacity measurements.*** The results of the magnetization measurements for one $Cu(Mo_xW_{1-x})O_4$ single crystal also characterized by a heat capacity measurement and neutron Laue diffraction are presented in detail. The mass of the crystal, hereafter named 'SC 300', is 30 mg and its dimensions are approximately $2.4 \cdot 1.7 \cdot 1$ mm^3 . The Mo-content of the crystal lies between 0.2 and 0.3, determined by a refinement based on single crystal x-ray data of several small crystal pieces obtained from near-surface regions. Figure 11 shows the magnetization vs. temperature along the easy axis with an applied magnetic field of $1/4\pi$ A/m (1 kOe). The Néel temperature, determined as the temperature of maximum slope, is 20(1) K. It is in accordance with the results of the heat capacity measurement at constant pressure (figure 12) indicating the magnetic phase transition from paramagnetic to antiferromagnetic in terms of a characteristic λ-peak, that is however anomalously broadened (see also section about single crystal neutron diffraction).

2.2.6 ***Single crystal neutron diffraction.*** The instrument VIVALDI [43] (Very Intense Vertical Axis Laue Diffractometer, ILL Grenoble, France) allows to investigate large volumes of reciprocal space simultaneously by using 'white', thermal neutrons of wavelengths from 0.7 to 5.2 Å.

The Laue diffraction patterns testify to the high quality of the crystal 'SC 300' without twinning and/or intergrowing of domains. Neither the $\frac{1}{2}$ 0 0-reflection nor the 0 0 $\frac{1}{2}$-reflection are visible in the Laue diffraction patterns at 2 K, implying that neither the $CuWO_4$- nor the $CuMoO_4$-III-type magnetic structure are realized.[1] Instead, a lot of other reflections exist that cannot be explained by the chemical structure and disappear on heating the sample above about 20 K, demonstrating their magnetic origin. Compared with the crystallographic reflections these magnetic reflections are severely broadened, i.e. the long-range magnetic order seems to be disturbed.

In order to correlate this magnetic structure with a magnetic coupling scheme, a model derived from the results of a spin dimer analysis of the anisotropic spin exchange interactions of the system's end members was applied. It is described in detail in [44, 45] and outlined here only in a summarized manner: In both end members the same two dimensional antiferromagnetic (2D AFM) sheets are built up by

[1] Overlap by the 1 0 0- or 0 0 1-reflections can be avoided by judicious choice of the rotation angle Φ of the crystal so that their exciting wavelengths lie outside the incident wavelength range.

the comparably strong super superexchange paths J_9(A), J_8, J_6(B) and the superexchange path J_1(A) (figure 13). Whereas these 2D AFM sheets couple via the superexchange path J_1(B) ferromagnetically in $CuWO_4$, leading to a magnetic unit cell with a doubled a axis in comparison with the chemical one, propagation vector $\vec{k}_W$=($\frac{1}{2}$, 0, 0), they couple antiferromagnetically in $CuMoO_4$-III, leading to a magnetic unit cell with a doubled c axis, propagation vector $\vec{k}_M$=(0, 0, $\frac{1}{2}$). Therefore, it is assumed that the 2D AFM sheets remain unchanged throughout the whole range of stoichiometries of the isomorphic solid solution series and that only the manner in which they couple between each other should change. The simplest extension of the magnetic coupling scheme for the intermediate stoichiometries, like the single crystal 'SC 300' exhibits, is built up of these 2D AFM sheets, which couple ferro- and antiferromagnetically in an alternating sequence (figure 14 (left)). This coupling scheme can equivalently be described as the formation of a relatively simple superstructure considering the sign of the magnetic exchange interaction of the J_1(B) superexchange paths (figure 14 (right)): This coupling scheme leads to a new magnetic structure—hereafter called 'WM-phase'—with a magnetic propagation vector $\vec{k}_{WM}$=($\frac{1}{4}$, $\frac{1}{2}$, $\frac{1}{4}$). Figure 15 shows some of sections of several Laue diffraction patterns for a variety of sample orientations at 2 K. All magnetic reflections of the whole series that are marked with P1 to P14 thereon can be explained by the model for the magnetic 'WM-phase' with propagation vector $\vec{k}_{WM}$=($\frac{1}{4}$, $\frac{1}{2}$, $\frac{1}{4}$). The correctness of the magnetic structure model resulting in this propagation vector is unambiguously confirmed by a preliminary diffraction experiment of the same crystal with monochromatic neutrons ($\lambda \approx 2.359\mathring{A}$) performed at the three axis diffractometer D10 (ILL, Grenoble). This experiment reveals that the streaking of the magnetic reflections, clearly visible already in the neutron Laue diffraction, is approximately along the $12\bar{1}$ reciprocal direction, which is approximately perpendicular to the 2D AFM sheets. The streaking is not a simple Lorentzian which would just reflect short-range correlation in the magnetic order perpendicular to the sheets, but is a combination of several incommensurate peaks, each of which may be Lorentzian along the $12\bar{1}$ direction. Exemplarily, figure 16 shows a projection of the observed counts along this direction through the reciprocal lattice point (0.23; 1.47; -0.68). A detailed temperature dependend analysis of the magnetic reflections with monochromatic neutrons and an interpretation with respect to the real structure will be subject of subsequent investigations. The anomalously broadened λ-peak of the heat capacity measurement already indicates that there seems not to be only one sharp magnetic phase transition from paramagnetic to antiferromagnetic within the whole crystal.

2.2.7 ***X-ray single crystal structure refinement.*** For a variety of stoichiometries single crystal x-ray structure refinements were performed at room temperature and for a selected Mo-content also at 200 K and 100 K. The data were collected with an XCalibur diffractometer with a CCD detector, the absorption correction was done by the programme package 'ABSSCALE' [46], and for the refinement the analysis software suite 'Crystals' [47] was used. Obtained results:

- The progression of the triclinic metric parameters and that of selected interatomic distances vs. stoichiometry does not give any obvious hints for the existence of any kind of discontinuity, and therfore an isosymmetric structural phase transition [48] at a certain stoichiometry can be excluded. Such a structural transition would have been consistent with the postulation of an accompanied sharp magnetic phase transition in [33]. The usage of stoichiometry dependent lattice parameters that are obtained from a linear interpolation between those for $CuWO_4$ and $CuMoO_4$-III is justified. This method was used for the representative analysis of the cation distribution obtained by Rietveld refinement based on high-resolution synchrotron diffraction data, but only based so far on the fact that the assumption is fulfilled by one crystal with $x = 0.25$ [49].
- In all refinements best reliability factors were obtained for a model with common Mo/W site with a constrained atomic position, anisotropic displacement factors and a refinable Mo/W ratio. The principal values of the thermal (Mo/W) displacement tensor for a variety of stoichiometries are all comparable in magnitude and orientation with the corresponding vector of the $CuWO_4$ end member, so that no indication for a split Mo/W site is given [50, 51].
- The temperature dependence of the root mean square value (r.m.s.) of the principal axis of the displacement ellipsoid was measured for a crystal with a relatively high Mo-content of $x = 0.45(1)$ to ensure

that the absolute scattering contribution of Mo is sufficiently large. In the case of a pure thermal oscillation contribution to the displacement factors, the r.m.s. should tend close to zero-point vibration when approaching 0 K [52]. Actually, for Cu as well as for Mo/W the same deviation from this progression can be observed experimentally: The principal axis displacements tend to higher values than expected for a pure thermal oscillation contribution. But, since this is observed for both, Cu and Mo/W atom sites, absorption effects and/or anharmonic contributions to the atom oscillations are more probable than static diplacements due to a split Mo/W-site.

- Many of the crystals, synthesized by chemical transport, were twinned. An investigation with a polarization light microscope revealed, that the outweighing part consists of only two domains. Two different kinds of twins have been found from diffraction experiments. The first twinning law corresponds to a two-fold axis along the crystallographic b axis, the second twinning law corresponds to a two-fold axis along the reciprocal b^* axis, i.e. a two-fold axis perpendicular to the a-c-plane.
- For a large variety of stoichiometries no super structure reflections stemming from a potential Mo/W ordering could be observed at room temperature.

3 Discussion

The results of the neutron Laue diffraction experiment, presented for the $Cu(Mo_xW_{1-x})O_4$ crystal 'SC 300' with x approximately 0.30 as representative, disproves the assumption of a sharp transition from the $CuWO_4$-(W-type) to the $CuMoO_4$-III-type (M-type) magnetic structure at a certain stoichiometry with increasing Mo-content around $x \approx 0.3$ as proposed in [33]. Instead, the magnetic reflections can be explained with a new magnetic structure, differing from those of the end members by the alternating sequence of ferro- and antiferromagnetically aligned two dimensional antiferromagnetic (2D AFM) sheets. This new magnetic phase also explains the results of the neutron powder diffraction experiments of the samples prepared by the Pechini method for $<x> = 0.25$, 0.30, and 0.35. In figure 17 the schematic magnetic phase diagram as a function of the stoichiometry x is extended by this additional 'WM-phase'. Since the Pechini samples possess a comparably narrow cation distribution, illustrated as narrow Gaussian distribution functions, the main part of the crystallites orders magnetically in the 'WM-phase' structure. Consequently, the sum of the refined scale factors of the magnetic end members reflects only a small fraction of the nuclear scale factor of the main phase that builds up the magnetic structure. In contrast, the samples prepared by subsolidus reaction possess a much broader cation distribution and only a considerably smaller amount of the crystallites orders in the 'WM-phase' structure. With respect to the restricted stoichiometric range of existence for the 'WM-phase' and the fact that its Néel temperature does not deviate substantially from the end members, it becomes also clear why a different sample preparation, affecting the homogeneity, causes different results for diffraction experiments but not for magnetization experiments. The existence of the 'WM-phase' cannot be derived from neutron powder diffraction, but by a single crystal experiment. The corresponding magnetic reflections are smeared out in the neutron Laue experiment, and in the light of their low intensity, it is hardly possible to detect them in powder diffraction. The alternating coupling scheme of the 2D AFM sheets can equivalently be described as the formation of a relatively simple super structure considering the sign of magnetic exchange interaction of the J_1(B) coupling paths, but it is not related to an accompanied formation of a super structure by an ordering of the Mo/W distribution. Such kind of ordering would result in super structure reflections due to the large difference of the x-ray scattering powers of W and Mo, but were not found in single crystal x-ray analysis for single crystals with stoichiometries in the critical region at room temperature. This means that the magnetic coupling scheme does not depend decisively on the specific occupation of neighbouring [(W, Mo)O_6] octahedra either with Mo or with W. The analyses of the single crystal x-ray diffraction data for a variety of stoichiometries supports that by not indicating any splitting of the Mo/W site. Rather, the statistical distribution of Mo/W induces, in terms of a cooperative process, the formation of a super structure determined by subtle structural details, that are nevertheless capable of changing the magnetic coupling scheme in the described manner.[1] However a super structure in

[1]The formation of super structures accompanied with changes in physical properties as a consequence of "chemical stress" induced by an elemental substitution is also well known for manganates $A_{1-x}B_xMnO_3$ (A: rare earth or alkaline earth metal ion; B: transition metal

the reported $Cu(Mo_xW_{1-x})O_4$ system can only be postulated indirectly within the assumption of a direct correlation of magnetic structure, magnetic coupling and local structural geometry [54]. At least at room temperature the results of the single crystal x-ray structure refinement for a variety of stoichiometries did not give an indisputable proof that a superstructure is realized already at this elevated temperature. Furthermore, the streaking of the magnetic reflection obtained from the detailed analysis of the single crystal neutron diffraction data that is interpreted as a combination of several incommensurate peaks and the anomalously broadened λ-peak found in the heat capacity measurement indicating that there seems not to be only one sharp magnetic phase transition from paramagnetic to antiferromagnetic are assumed to be related to the the specific Mo/W distribution, i.e. the concentration fluctuations on a macroscopic scale revealed by the chemical analyses. The more detailed investigation of this peculiar observations will be subject of subsequent investigations concerning the effect of the real structure on the magnetic properties of the solid solution series. However, the crystal lattice distortions found in the TEM analyses are supposed to have a negligible effects on the magnetic properties.

4 Conclusions

The particular local occupation with W or Mo in the $Cu(Mo_xW_{1-x})O_4$ solid solution, that is statistical in general, does not result in a corresponding statistical spatial distribution of ferro- or antiferromagnetically coupling exchange paths, respectively, that would have resulted in a magnetically frustrated system. From all experimental results it can be inferred that cooperative processes are dominant, i.e. depending on the overall Mo/W ratio the statistical distribution leads to the formation of a three dimensional periodic magnetic coupling scheme. Whereas in $CuWO_4$ and $CuMoO_4$-III the decisive $J_1(B)$ exchange path couples exclusively ferro- and antiferromagentically, respectively, in the solid solution series of a certain stoichiometry range about $x \approx 0.3$ a superstructure consisting of both coupling types is built up. Within the assumption of a direct correlation of magnetic coupling type and local structural geometry, appropriate for this system with localized electrons, a crystal structure obtained theoretically from a linear interpolation of the end members' structure seems to be energetically unfavorable. Instead, a simple super structure, consisting of structural elements with bonding geometries typical for the end members, respectively, is realized. The magnetic properties act here as a very sensitive probe for these subtle structural modulations. This example shows further that very sophisticated structural and local chemical analyses are essential for the interpretation of physical properties of solid solution crystals, especially with respect to local interactions.

Acknowledgement

We would like to thank Dr. C. Meingast and Dr. W. Knafo from the Forschungszentrum Karlsruhe for the heat capacity measurements. Financial support by the Deutsche Forschungsgemeinschaft (WE 1542/5-3) is gratefully acknowledged.

References

[1] P.W. Anderson, Phys. Rev. **79** 350 (1950).
[2] P.J. Hay, K.C. Thibeault, R. Hoffmann, J. Am. Chem. Soc. **97** 4884 (1975).
[3] H. Dachs, E. Stoll, H. Weitzel, Z. Kristallogr. **125** 120 (1967).
[4] D. Uelkue, Z. Kristallogr. **124** 192 (1967).
[5] H. Weitzel, Z. Kristallgr. **144** 238 (1976).
[6] R.O. Keeling, Acta Cryst. **10** 209 (1957).
[7] J. Kanamori, J. Appl. Phys. **31** 14 (1960).
[8] L. Kihlborg, E. Gebert, Acta Cryst. B **26** 1020 (1970).
[9] L.G. VanUitert, R.B. Soden, J. Appl. Phys. **31** 328 (1964).
[10] S.K. Arora, T. Mathew, N.M. Batra, J. Phys. Chem. Solids **50** 665 (1989).
[11] S.K. Arora, T. Mathew, Phys. Stat. Solidi (a) **116** 405 (1989).

ion) [53].

[12] S.K. Arora, T. Mathew, N.M. Batra, J. Phys. D **23** 460 (1990).
[13] T. Mathew, N.M. Batra, S.K. Arora, J. Mater. Sci. **27** 4003 (1992).
[14] A.K. Basu, F.R. Sale, J. Mater Sci. **13** 91 (1979).
[15] J.P. Doumerc, J. Hejtmanek, J.P. Chaminade, M. Pouchard, M. Krussanova, Phys, Stat. Solidi (a) **82** 285 (1984).
[16] S.K. Arora, T. Mathew, B. Chudasama, A. Kothari, J. Cryst. Growth **275** e651-e656 (2005).
[17] B. Lake, D.A. Tennant, R.A. Cowley, J.D. Axe, C.K. Chen, J. Phys.: Condens. Matter **8** 8613 (1996).
[18] B. Lake, R.A. Cowley, D.A. Tennant, J. Phys.: Condens. Matter **9** 10951 (1997).
[19] B. Lake, D.A. Tennant, Physica B **234-6** 557 (1997).
[20] A.G. Anders, A.I. Zvyagin, Sov. Phys. JETP **36** 1151 (1973).
[21] A.I. Zvyagin, A.G. Anders, Sov. Phys. JETP **40** 154 (1975).
[22] J.B. Forsyth, C. Wilkinson, A.I. Zvyagin, J. Phys.: Condens. Matter **3** 8433 (1991).
[23] A.G. Anders, A.I. Zvyagin, M.I. Kobelts, L.N. Pelikh, E.N. Khats'ko, V.G. Yurko, Sov. Phys. JETP **35** 934 (1972).
[24] J.P. Doumerc, J.M. Dance, J.P. Chaminade, M. Pouchard, P. Hagenmuller, M. Krussanova, Mater. Res. Bull. **16** 985 (1981).
[25] H. Weitzel, Solid State Commun. **8** 2071 (1970).
[26] H. Weitzel, H. Langhof, J. Magn. Magn. Mater. **4** 265 (1977).
[27] S.C. Abrahams, J.L. Bernstein, P.B. Jamieson, J. Chem. Phys. **48** 2619 (1968).
[28] A.W. Sleight, Mater. Res. Bull. **8** 863 (1973).
[29] R. Tali, V.V. Tabachenko, L.M. Kovba, L.N. Dem'yanets, Russ. J. Inorg. Chem. **36** 927 (1991).
[30] M. Wiesmann, H. Ehrenberg, G. Miehe, T. Peun, H. Weitzel, H. Fuess, J. Solid State Chem. **132** 88 (1997).
[31] A.P. Young, C.M. Schwartz, Science **141** 348 (1963).
[32] H. Ehrenberg, M. Wiesmann, J. Garcia-Jaca, H. Weitzel, H. Fuess, J. Magn. Magn. Mater. **182** 152 (1998).
[33] H. Ehrenberg, R. Theissmann, Y. Gassenbauer, M. Knapp, G. Wltschek, H. Weitzel, H. Fuess, T. Herrmannsdoerfer, D. Sheptyakov, J. Phys.: Condens. Matter **14** 8573 (2002).
[34] M.P. Pechini, US Patent. 3330697 (1967).
[35] H.M. Rietveld, J. Appl. Cryst. **2** 65 (1969).
[36] H. Ehrenberg, H. Weitzel, H. Paulus, M. Wiesmann, G. Wltschek, M. Geselle, H. Fuess, J. Phys. Chem. Sol. **58** 153 (1997).
[37] J. Roisnel, J.Rodriguez-Carvajal, WinPLOTR: A Windows tool for Powder Diffraction Pattern Analysis.
[38] Y. Fuju, U. Schanz, E. Schmidbauer, J. cryst. growth **132** 606 (1993).
[39] R. Neddermann, S. Gerighausen, M. Binnewies, Z. anorg. allg. Chem. **622** 21 (1995).
[40] M. Brinkmann, Dissertation, Fakultät für Physik und Astronomie an der Ruhr-Universität Bochum, Bochum (1997).
[41] A.R. Drews, M.S. Osofsky, H.A. Hoff, J.L. Peng, Z.Y. Li, R.L. Greene, T.A. Vanderah, Physica C **200** 122 (1992).
[42] E.F. Skelton, A.R. Drews, M.S. Osofsky, S.B. Qadri, J.Z. Hu, T.A. Vanderah, J.L. Peng, R.L. Greene, Science **263** 1416 (1994).
[43] G.J. McIntyre, M.H. Lemee-Cailleau, C. Wilkinson, Physica B **1005** 385 (2006).
[44] H.-J. Koo, M.-H. Whangbo, Inorg. Chem. **40** 2161 (2001).
[45] B. Schwarz, H. Ehrenberg, H. Weitzel, H. Fuess, Inorg. Chem. **46** 378 (2007).
[46] Oxford Diffraction Poland. Oxford Diffraction Ltd., Xcalibur CCD System, CrysAlis Software System, Version 1.171.27. (2005).
[47] P.W. Betteridge, J.R. Carruthers, R.I. Cooper, K. Prout, D.J. Watkin, J. Appl. Cryst. **36** 1487 (2003).
[48] A.G. Christy, Acta Cryst. **B51** 753 (1995).
[49] M. Knapp, Dissertation, Fachbereich Material- und Geowissenschaften, TU Darmstadt (2002).
[50] B. Schwarz, Dissertation, Fachbereich Material- und Geowissenschaften, TU Darmstadt (2007).
[51] R.T. Downs, Reviews in Mineralogy and Geochemistry V. **41** (2000).
[52] H. Boysen, Z. Kristallogr. **18** 123 (2003).
[53] H.Y. Hwang, S.W. Cheong, P.G. Radaelli, M. Marezio, B. Batlogg, Phys. Rev. Lett. **75** 914 (1995).
[54] J. Kanamori, J. Phys. Chem. Sol. **10** 87 (1959).

- Figure1: Sections of high resolution synchrotron x-ray powder diffractograms of $Cu(Mo_xW_{1-x})O_4$ samples with $<x> = 0.25$. Compared are the data of the sample prepared by subsolidus reaction (top) and by the Pechini method (bottom). The red circles are the measured points, the black line is the calculated diffractogram, the blue line at the bottom are their difference plot and the green markers represent the positions of the reflections with varying Mo-content, starting with $x = 0$ at the top and $\Delta x = 0.05$ for each subsequent row.
- Figure2: Cation distribution function, as deduced from high-resolution synchrotron diffraction data, for two samples prepared by different methods, namely by subsolidus reaction and by the Pechini method, but with the same averaged composition $<x> = 0.25$. The relative amounts are approximately proportional to the scale factors of discrete compositions used to approximate the continuous functions.
- Figure3: Sections of high resolution synchrotron x-ray powder diffractograms of $Cu(Mo_xW_{1-x})O_4$ samples with $<x> = 0.25$, 0.30, 0.35 and 0.50. Especially for $x > 0.3$ the anomalies in the reflection profiles related to distinct Mo-contents are very pronounced as indicated by arrows. A small part of crystallites of these samples has lost Mo due to the formation of the Mo-rich γ-$Cu(Mo_xW_{1-x})O_4$ phase.
- Figure4: Néel temperature vs. stoichiometry $<x>$, determined as the temperatures of maximum slope from the magnetization vs. temperature measurements for a variety of stoichiometries from $<x> = 0$ to $<x> = 0.4$.
- Figure5: Sections of neutron powder diffractograms showing the strongest magnetic reflections of the magnetic $CuWO_4$-type (left marker) and the $CuMoO_4$-III-type (right marker) structures. Left: The samples prepared by subsolidus reaction for the averaged stoichiometries $<x> = 0.15$, 0.25 and 0.35 were measured at CMD (PSI, Switzerland). Right: The samples prepared by the Pechini method for the stoichiometries $<x> = 0.00$, 0.25, 0.30 and 0.35 were measured at SPODI (FRM II, Germany).
- Figure6: Left: Exemplarily chosen spatial Mo distribution obtained from a line scan over the whole crystal surface. Right: Atomic elemental concentrations that were used to obtain the Mo distribution presented in the left part of this figure. The alternating fluctuations of the W- and Mo-concentration in opposite direction together with an approximately constant Cu- and O-concentration demonstrate that the observed fluctuations are a real effect.
- Figure7: X-ray q-scans of the reflections 002, 200 and $0\bar{2}0$.
- Figure8: X-ray q-scans of the reflections 400, $0\bar{4}0$, 004, 130 and 220.
- Figure9: Left: High resolution TEM bright-field image of an imperfection. Middle: A horizontal compression of the image on the left to 10 %. Right: A magnification of the image in the middle.
- Figure10: High resolution TEM bright-field image parallel to [00±1] of the $Cu(Mo_xW_{1-x})O_4$ single crystal 'SC ID' showing multi-twinning crystal domain relations.
- Figure11: Magnetization vs. temperature for the $Cu(Mo_xW_{1-x})O_4$ single crystal 'SC 300' at a magnetic field of $1/4\pi$ A/m (1000 Oe).
- Figure12: Heat capacity C_p vs. temperature for the $Cu(Mo_xW_{1-x})O_4$ single crystal 'SC 300'. Left: C_p with estimated standard deviations and $\left(\frac{T}{\theta}\right)^3$-fit for the nuclear part of the heat capacity. Middle: Difference of heat capacity and $\left(\frac{T}{\theta}\right)^3$-fit. Right: Magnification of the image of the middle.
- Figure13: Perspective view on a 2D AFM sheet, existing in the $CuWO_4$- as well as in $CuMoO_4$-III-type magnetic structure. The filled and unfilled circles represent spin-up and spin-down, respectively.
- Figure14: Arrangement of the Cu^{2+} ions for the magnetic structure postulated for the critical region of stoichiometry around $x = 0.3$. The filled and unfilled circles represent spin-up and spin-down, respectively. Left: The 2D AFM sheets in horizontal orientation are highlighted by black connection lines. They couple ferro- (dashed blue) and antiferromagnetically (red) via the J_1(B) coupling path in an alternating sequence. Right: From another perspective it becomes clear that the coupling scheme can equivalently be described as a super structure considering the sign of the magnetic exchange interaction of the J_1(B) coupling paths. The unit cell of this super structure is marked with a solid lined box. The chemical unit cell of the end members is marked with a dotted lined box.
- Figure15: A selection of sections of neutron Laue diffraction patterns of the $Cu(Mo_xW_{1-x})O_4$ single crystal 'SC 300' at 2 K for varying sample orientations. All magnetic reflections of the whole series are labelled with P1 to P14. Only a part of them is presented here.
- Figure16: Projection of the observed counts along the $12\bar{1}$ direction through the reciprocal lattice point

(0.23; 1.47; -0.68) obtained by monochromatic ($\lambda = 2.359\mathring{A}$) neutron diffraction for the $Cu(Mo_xW_{1-x})O_4$ single crystal 'SC 300'.

- Figure17: Schematic magnetic phase diagram with the additional new magnetic 'WM-phase' for x about 0.3. The stoichiometric distribution functions of the samples prepared by subsolidus reaction are sketched in by broad Gaussian functions (dashed line), those of the Pechini samples by narrower ones (solid line).

Figure 1.

Figure 2.

Figure 3.

Figure 4.

Figure 5.

Figure 6.

Figure 7.

Figure 8.

Figure 9.

Figure 10.

Figure 11.

Figure 12.

Figure 13.

Figure 14.

Figure 15.

Figure 16.

Figure 17.

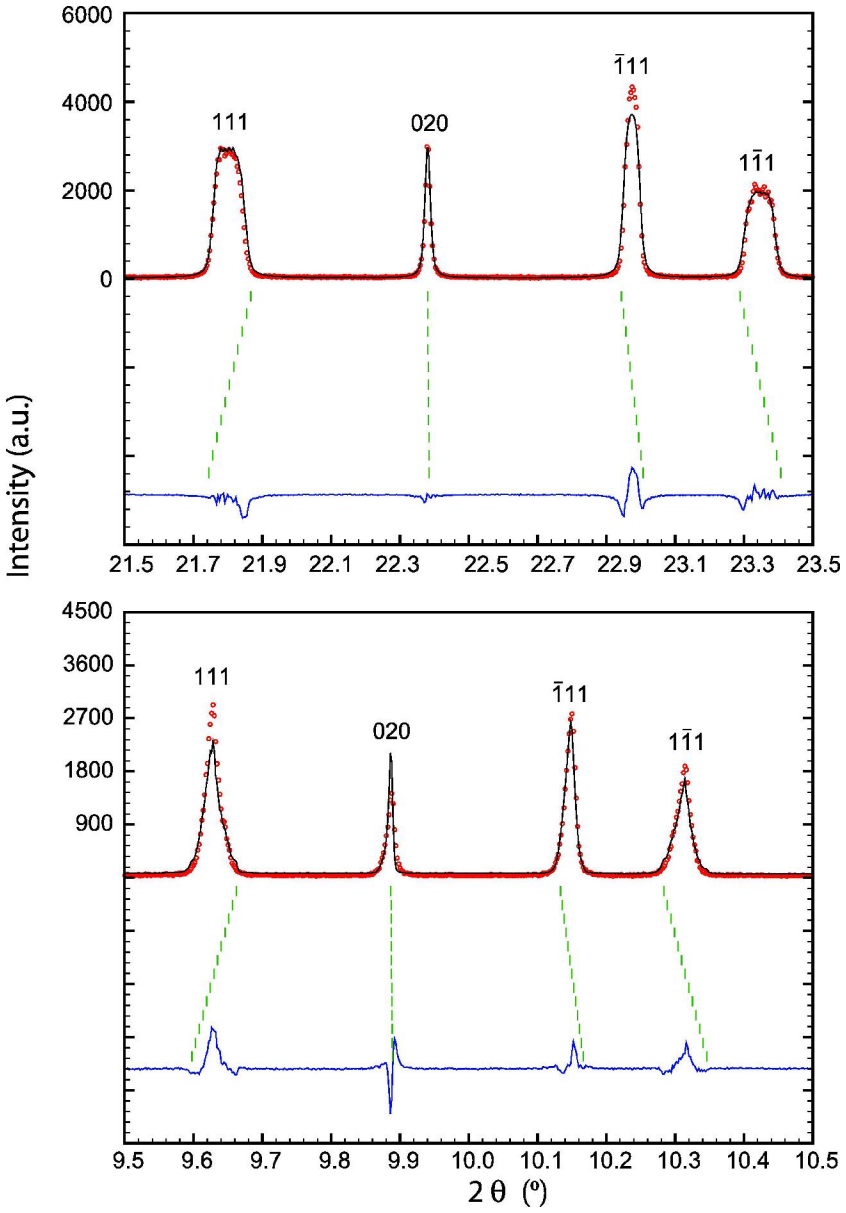

116x168mm (600 x 600 DPI)

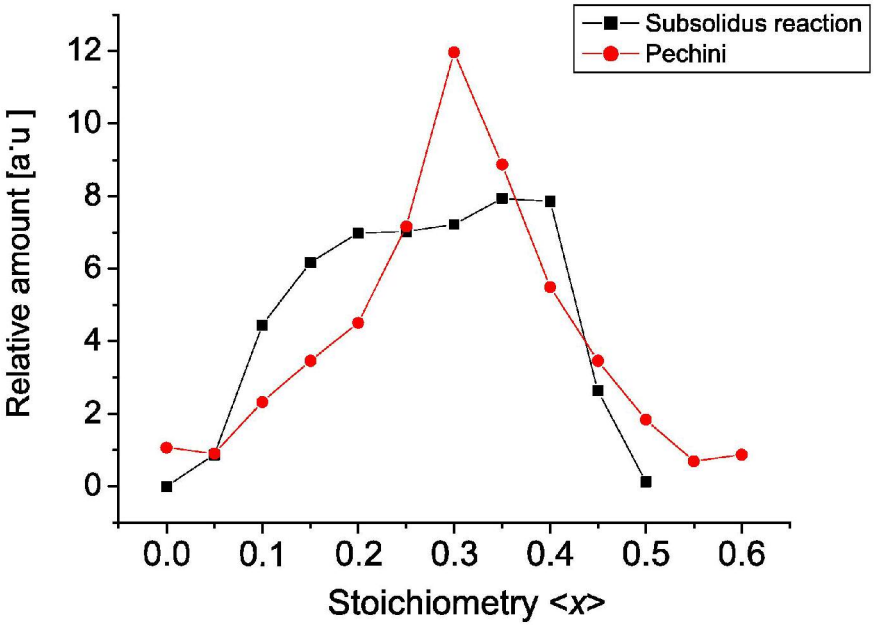

82x61mm (600 x 600 DPI)

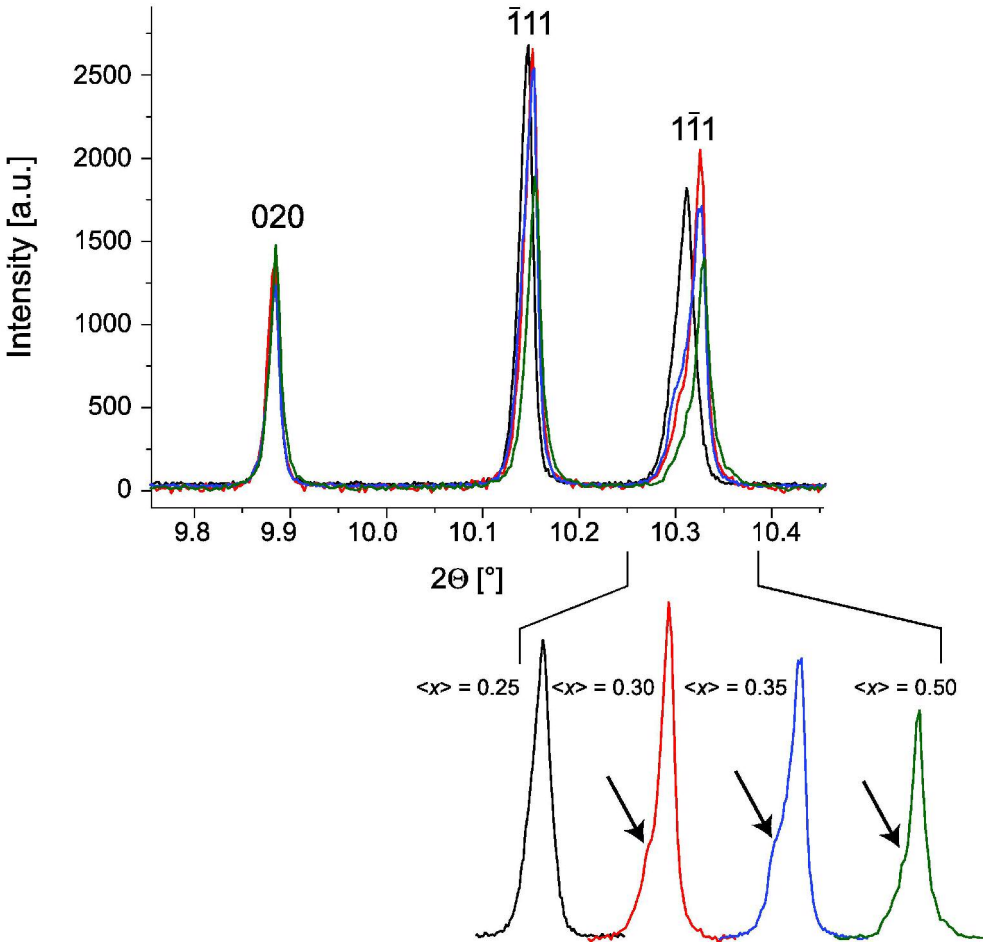

108x112mm (600 x 600 DPI)

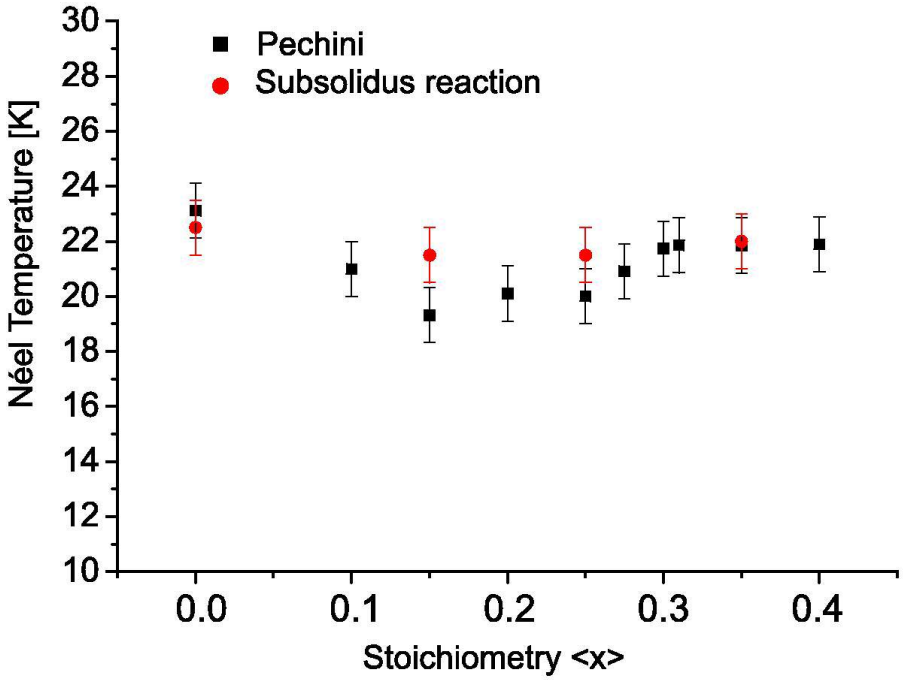

56x45mm (600 x 600 DPI)

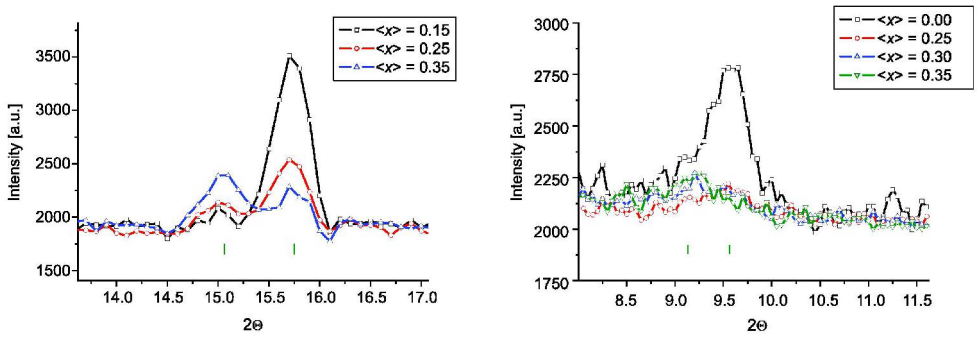

108x41mm (600 x 600 DPI)

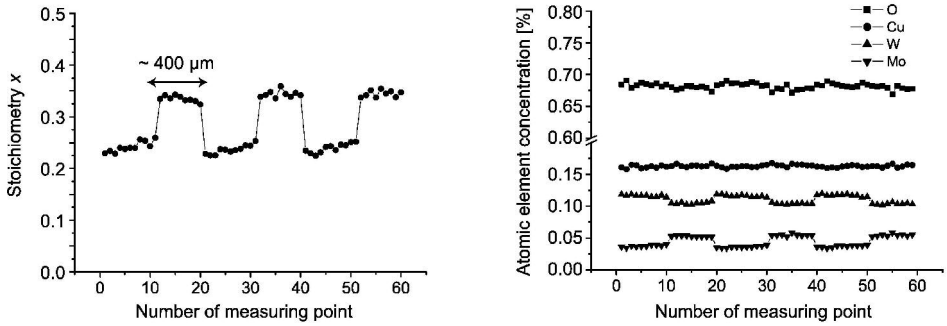

152x57mm (600 x 600 DPI)

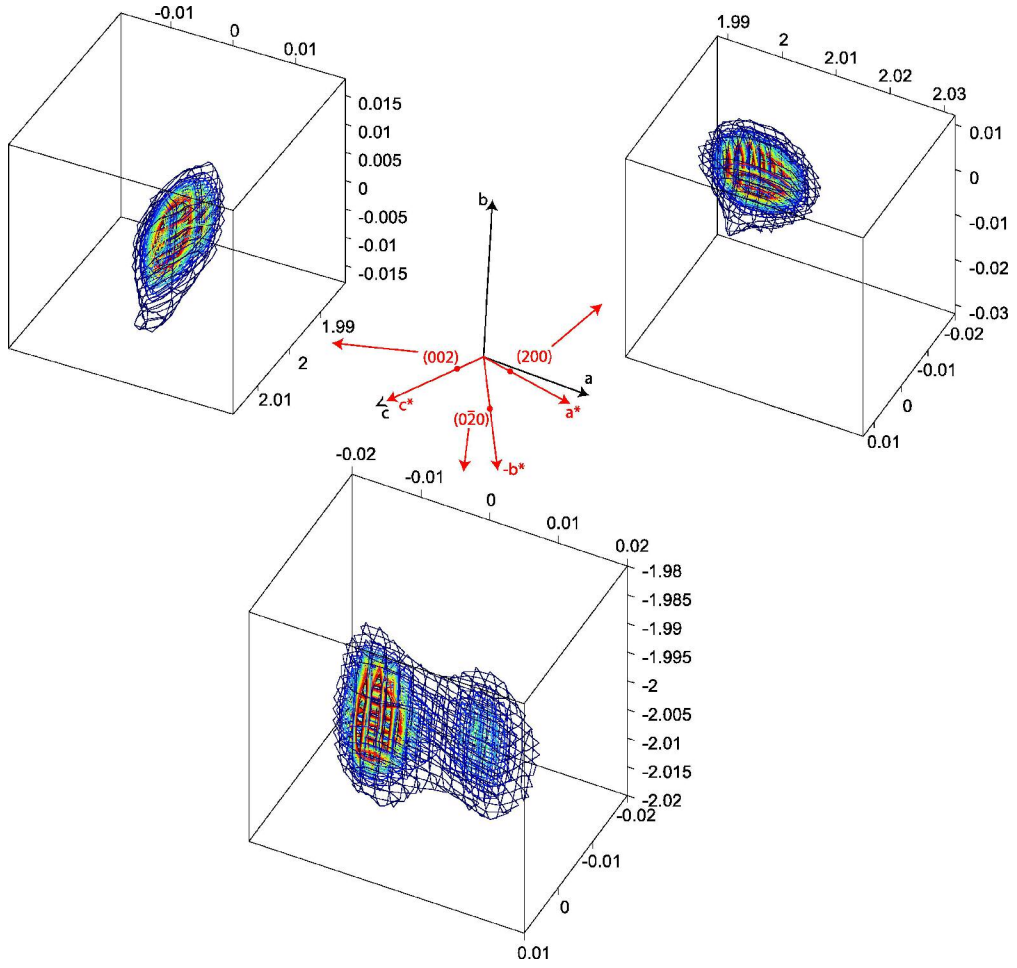

138x132mm (600 x 600 DPI)

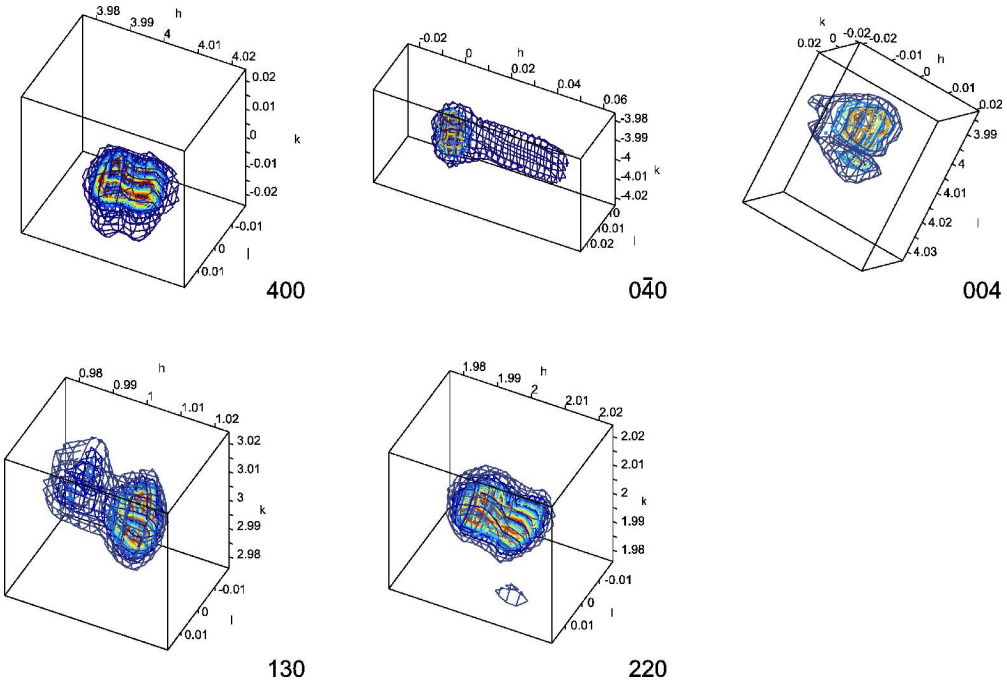

172x115mm (600 x 600 DPI)

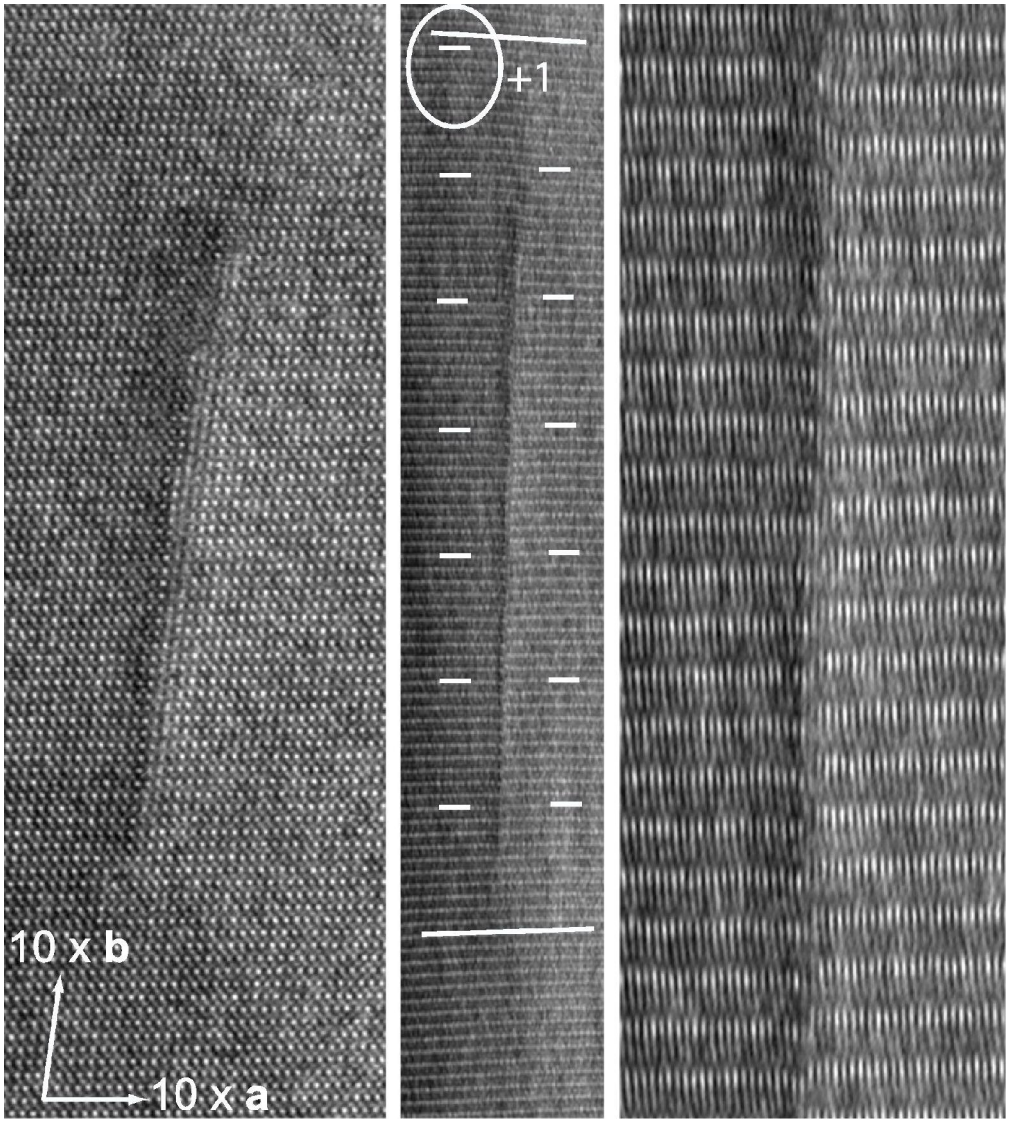

80x89mm (600 x 600 DPI)

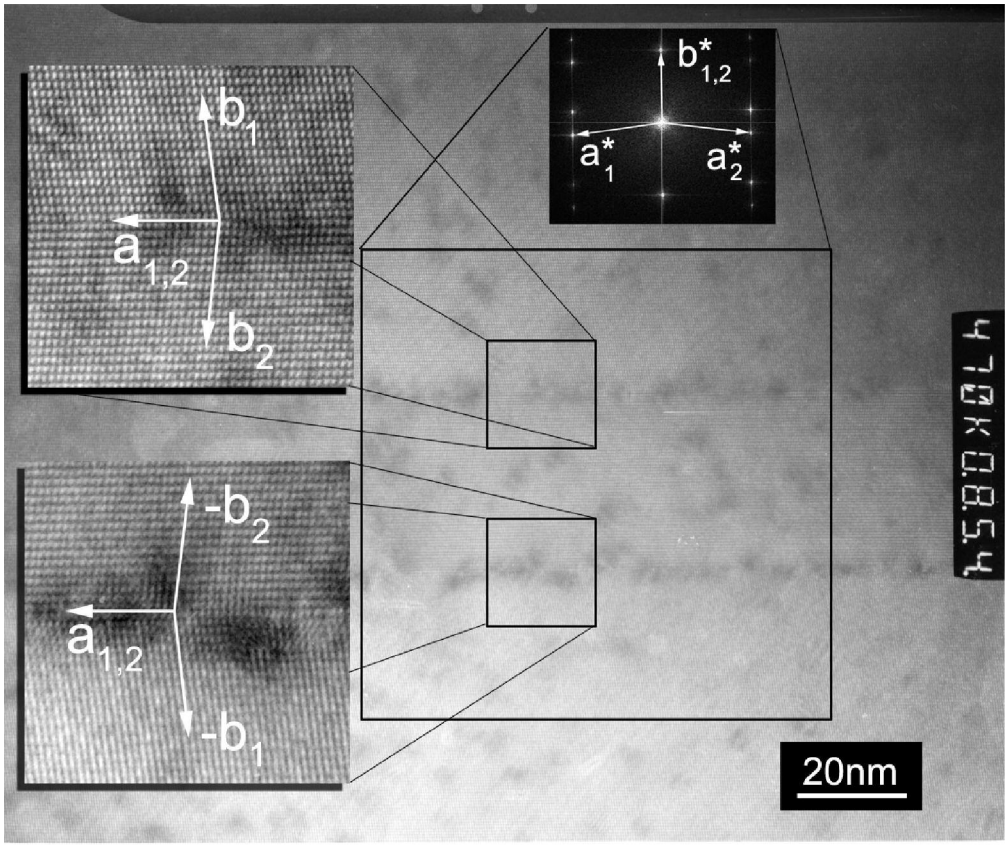

92x77mm (600 x 600 DPI)

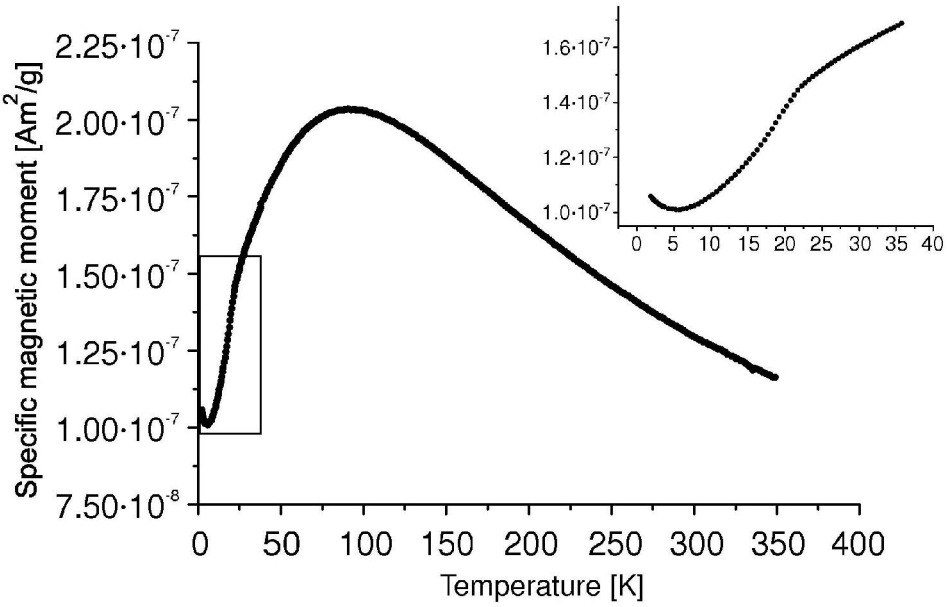

84x57mm (600 x 600 DPI)

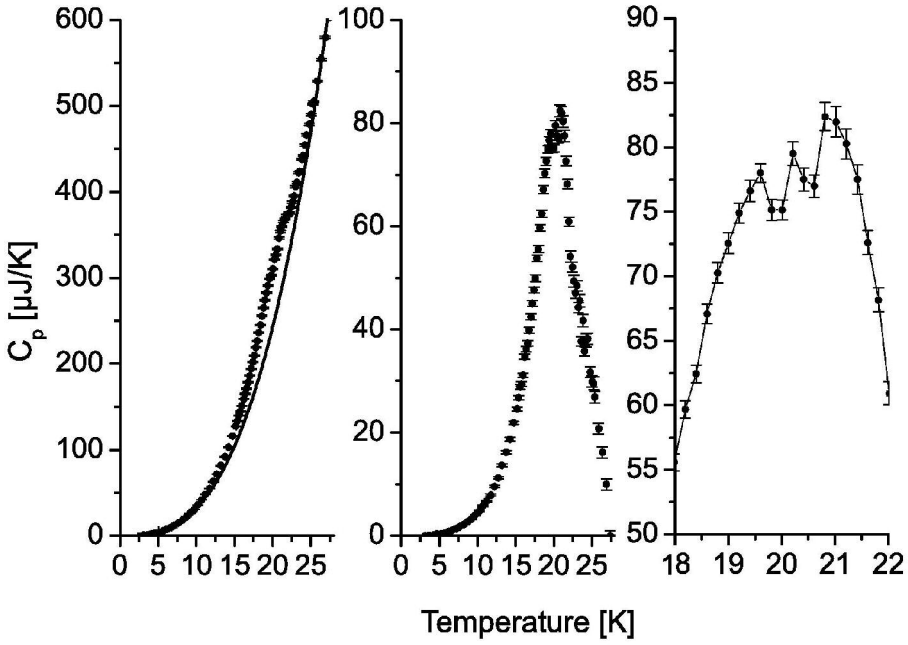

79x58mm (600 x 600 DPI)

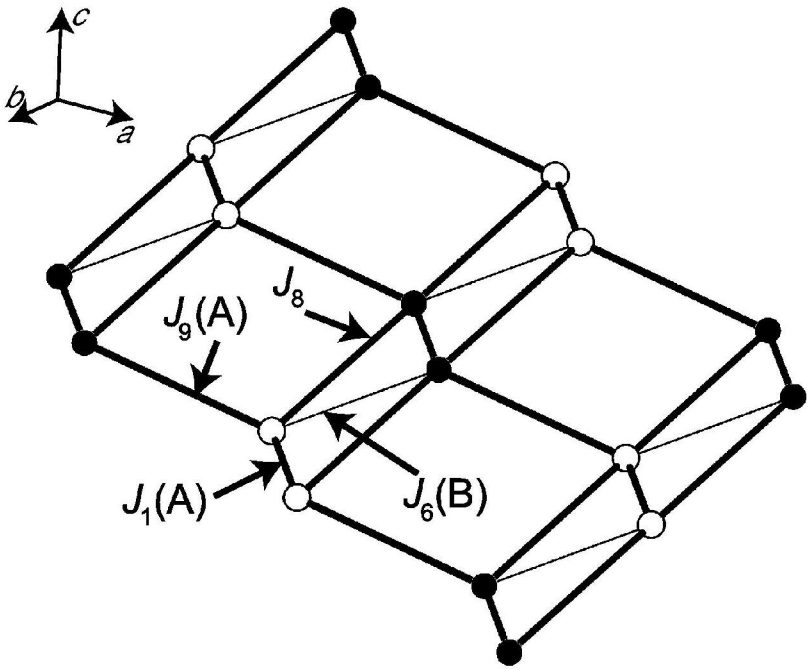

77x57mm (600 x 600 DPI)

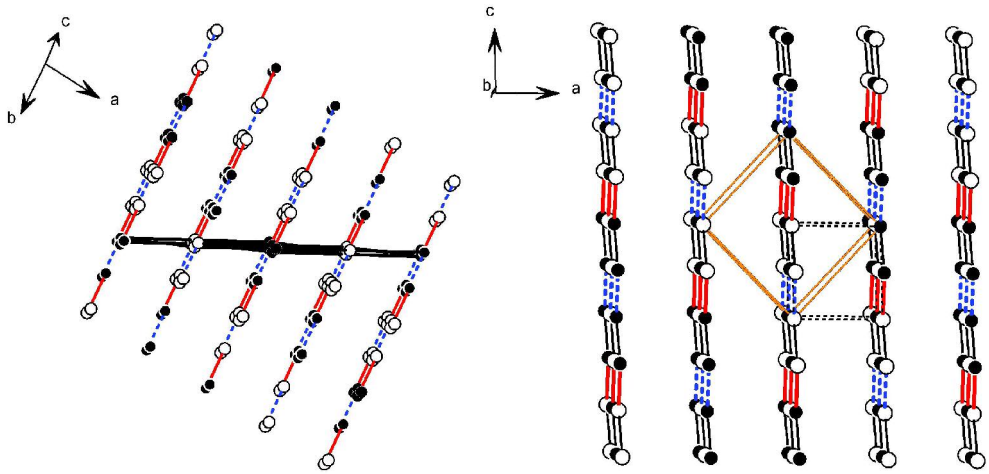

119x59mm (600 x 600 DPI)

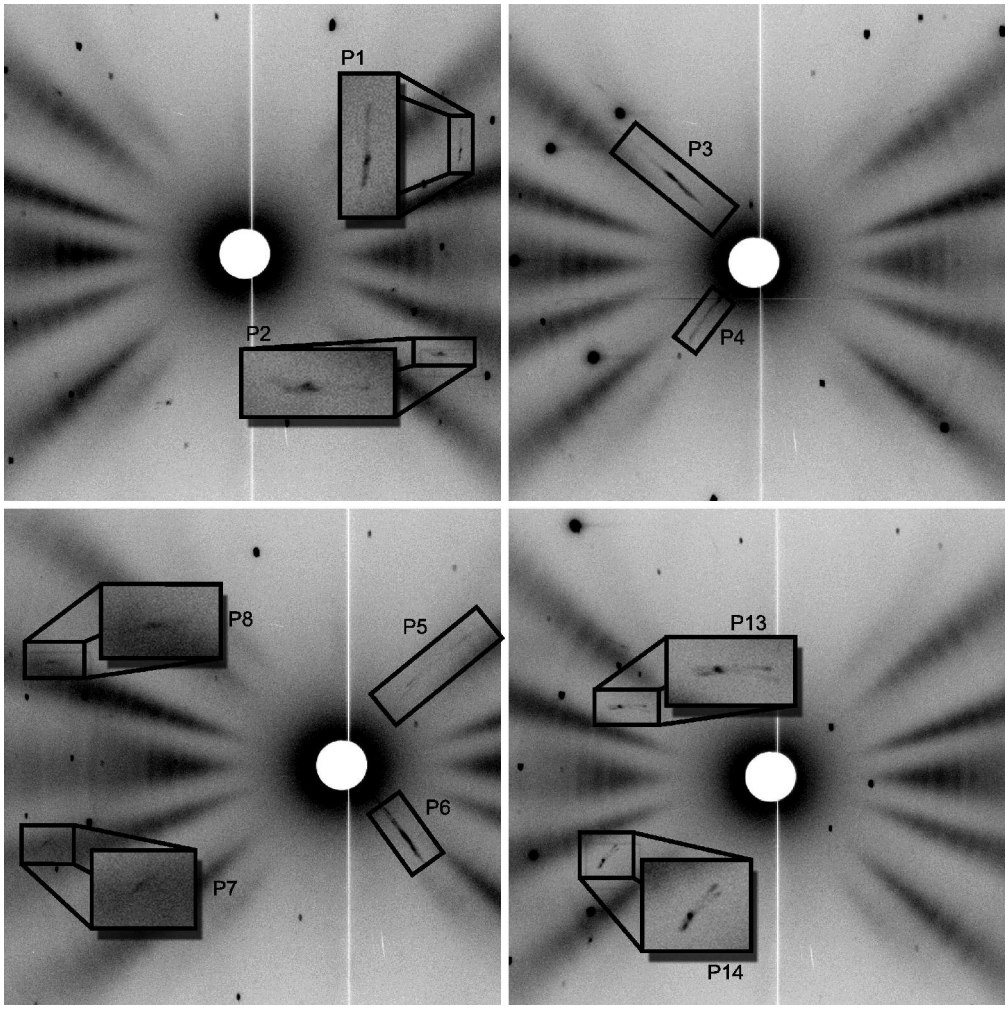

108x108mm (600 x 600 DPI)

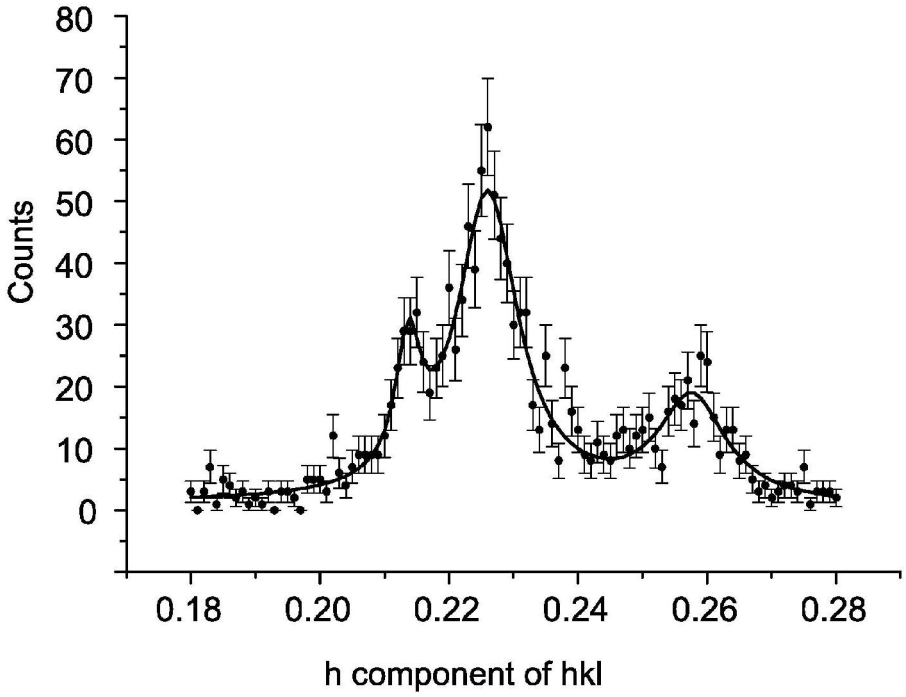

81x65mm (600 x 600 DPI)

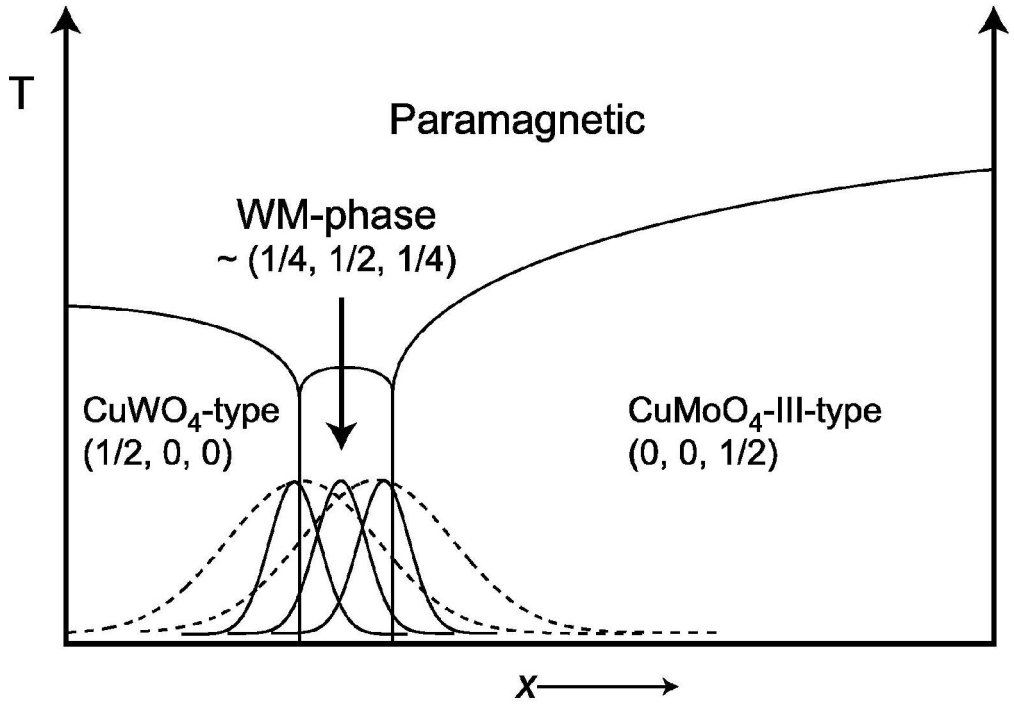

71x50mm (600 x 600 DPI)